Superfluid to normal phase transition in strongly correlated bosons in two and three dimensions

Juan Carrasquilla and Marcos Rigol

Department of Physics, Georgetown University, Washington, D.C. 20057, USA and
Physics Department, The Pennsylvania State University, 104 Davey Laboratory, University Park, Pennsylvania 16802, USA

Using quantum Monte Carlo simulations, we investigate the finite-temperature phase diagram of hard-core bosons (*XY* model) in two- and three-dimensional lattices. To determine the phase boundaries, we perform a finite-size-scaling analysis of the condensate fraction and/or the superfluid stiffness. We then discuss how these phase diagrams can be measured in experiments with trapped ultracold gases, where the systems are inhomogeneous. For that, we introduce a method based on the measurement of the zero-momentum occupation, which is adequate for experiments dealing with both homogeneous and trapped systems, and compare it with previously proposed approaches.

I. INTRODUCTION

The description of strongly correlated bosonic systems is of fundamental interest in largely diverse physical situations ranging from low-temperature experiments with superfluid helium [1] to Josephson-junction arrays [2], as well as magnetic insulators [3] and ultracold gases in optical lattices [4,5]. The latter systems offer an unparalleled playground to study fundamental models widely considered in statistical and condensed matter physics. This is because of the high degree of control over the experimental parameters that determine the Hamiltonian describing the system. In particular, the Bose-Hubbard model [6,7] has been experimentally realized in one [8], two [9,10], and three dimensions [11], where the superfluid to Mott insulator transition has been observed. Even though it has received less attention, the superfluid to normal transition in the Bose-Hubbard model has been investigated experimentally in three dimensions [12], while in two dimensions it has been realized in the form of a two-dimensional lattice of Josephson-coupled Bose-Einstein condensates [13,14] as well as in experiments with ultracold atoms in optical lattices [15].

Although experiments with ultracold atoms on optical lattices are in some respects almost ideal realizations of model Hamiltonians of interest, significant complications arise because of the presence of a confining potential, which leads to the coexistence of different phases in a single experimental setup [16,17]. Furthermore, the mesoscopic size of the system in combination with the inhomogeneity induced by the trapping potential produces a rounding off of the otherwise sharp features present in an infinite homogeneous system in the critical region [18–21]. Thus the understanding and assessment of criticality in such systems remains a challenging task.

The emergence of sharp features in the momentum distribution as obtained from time-of-flight images has been frequently associated to the emergence of superfluidity [11,22–25]. However, this association may not be accurate because sharp peaks in the momentum distribution already appear in the normal state, due to an increasing correlation length when approaching a critical regime [26–28]. More recently, new schemes to detect criticality in trapped systems have been proposed. In some of those studies, a detailed analysis of the momentum distribution was used to define criteria that allow

one to extract reliable estimations of the critical points from time-of-flight images [12,27,29]. In addition to time-of-flight images, high-resolution *in situ* imaging of the density profile of trapped systems has become a powerful instrument with which one can also study phase diagrams of strongly correlated systems and quantum criticality. Numerous theoretical and experimental studies based on this idea have been carried out for systems in the presence of an optical lattice [30–40] and in the absence of it [41–44].

One important aspect that determines the nature of the quantum phases and their associated order parameters is the dimensionality *d*. Mermin *et al.* rigorously proved that at any nonzero temperature, continuous symmetries cannot be spontaneously broken in systems with sufficiently short-range interactions in dimensions $d \leqslant 2$ [45,46]. This implies that, at finite temperature, Bose-Einstein condensation (BEC) cannot occur in one and two dimensions. Two-dimensional Bose systems, however, are marginal in the sense that fluctuations are strong enough to destroy the fully ordered state, but are not so strong as to suppress superfluidity. Thus critical behavior develops in the Berezinskii-Kosterlitz-Thouless (BKT) transition [47,48], where a superfluid phase with quasi-long-range order competes with thermal fluctuations and induces a continuous phase transition to the normal fluid as the temperature is increased. In addition to low-temperature superfluidity, long-range order can develop at zero temperature in two dimensions. On the other hand, in three dimensions, the superfluid transition is accompanied by the appearance of true long-range order, implying that the system also exhibits Bose-Einstein condensation. Such a transition, which belongs to the three-dimensional *XY* universality class, is well understood in the sense that the critical exponents have been determined experimentally and theoretically with remarkably high accuracy in many different physical contexts [49–55].

Here, we focus our study on the superfluid to normal transition in a system of strongly interacting bosons in two- and three-dimensional lattices. Specifically, we consider the Bose-Hubbard model in the limit of infinite on-site repulsion, i.e., the hard-core boson limit. We use exact quantum Monte Carlo simulations to compute the finite-temperature phase diagram as a function of chemical potential. Accurate results are obtained through finite-size scaling of the condensate

fraction and/or the superfluid stiffness obtained from our simulations. We also determine the mean-field phase diagram, which is qualitatively correct but quantitatively quite different from the exact results. We then proceed to study the superfluid to normal phase transition in two and three dimensions in the presence of a confining potential, which is required to describe experiments with ultracold gases. We introduce a method to determine the critical temperature, for any given density, that is based on the measurement of the zero-momentum occupation as a function of temperature. This method is in principle adequate for experiments dealing with both homogeneous and trapped systems. Furthermore, we compare our approach to other recently proposed schemes based on the *in situ* density images [31] as well as on the shape of the low-momentum part of the momentum distribution. [29]

The paper is organized as follows. In Sec. II, we introduce the model and its phase diagram in two and three dimensions supplemented with the mean-field calculations. Section III is devoted to the discussion of the techniques to obtain the phase boundaries. In Sec. IV, we discuss the possibility to have Bose-Einstein condensation in trapped two-dimensional systems, as well as the methods to determine the phase boundaries from experimentally accessible quantities. Finally, in Sec. V, we draw our conclusions.

II. MODEL AND PHASE DIAGRAM

We consider a system of hard-core bosons on a d-dimensional lattice with L^d sites. The Hamiltonian can be written as

$$\hat{H} = -t \sum_{\langle i,j \rangle} (\hat{a}_i^\dagger \hat{a}_j + \text{H.c.}) - \sum_i \mu_i \hat{n}_i, \qquad (1)$$

where $\hat{a}_i^\dagger$ ($\hat{a}_i$) is the boson creation (annihilation) operator at a given site i, and $\hat{n}_i = \hat{a}_i^\dagger \hat{a}_i$ is the local particle-number operator. The hard-core boson creation and annihilation operators satisfy the constraint $\hat{a}_i^{\dagger 2} = \hat{a}_i^2 = 0$, which forbids multiple occupancy of lattice sites. The first term in Eq. (1) is the kinetic energy, where t is the hopping amplitude between neighboring sites i and j ($\langle i,j \rangle$). In experiments involving ultracold gases, a trap is required to confine the atoms. The effect is taken into account in the second term that contains $\mu_i = \mu - V_0 r_i^2$, where V_0 is its strength and μ is the overall chemical potential. r_i is the distance from site i to the center of the trap. In what follows, positions will be given in units of the lattice spacing a and the energy will be given in units of the hopping amplitude t.

We recall that the Hamiltonian in Eq. (1) can be exactly mapped to the extensively studied quantum XY model [56],

$$\hat{H} = -2t \sum_{\langle i,j \rangle} \left(S_i^x S_j^x + S_i^y S_j^y \right) - \sum_i \mu_i S_i^z, \qquad (2)$$

where S_i^α is the αth component of the spin-1/2 spin operator at site i. In the spin language, the term proportional to t describes a ferromagnetic exchange interaction, while the one proportional to μ_i describes a magnetic field in the z direction at site i.

We study the Hamiltonian in Eq. (1), at finite temperature T, by means of the stochastic series expansion (SSE)
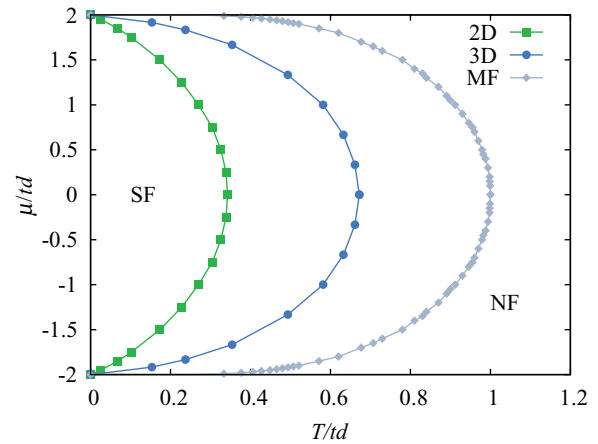
FIG. 1. (Color online) Finite-temperature phase diagram in two and three dimensions, and the mean-field (MF) prediction. In all dimensions, the phase diagram contains a superfluid (SF) lobe surrounded by the normal fluid (NF) phase.

quantum Monte Carlo (QMC) method with operator-loop updates [57–59]. The determination of the phase diagrams is carried out through a finite-size scaling of the condensate fraction and/or the superfluid stiffness ρ_s using periodic boundary conditions. The numerically exact (QMC) phase diagram in two dimensions (2D) and three dimensions, as well as the the mean-field predictions, are presented in Fig. 1. The finite-temperature phase diagram comprises an off-diagonal long-range-ordered (ODLRO) low-temperature superfluid lobe (quasi-ODLRO in 2D) surrounded by a high-temperature normal phase with exponentially decaying correlation functions. The extend of the superfluid state is expected to be hindered as dimensionality is reduced because thermal and quantum fluctuations have a stronger effect in low-dimensional systems. Clearly, our results agree with that expectation. The dissimilarity between the mean-field and the exact phase diagrams makes it clear that both thermal and quantum fluctuations are strong and play an important role even in three dimensions, where mean-field approaches are generally considered to be a good approximation.

Details on the procedure to obtain the phase boundaries are provided in the following sections. Such procedures are different in two and three dimensions because of the different universality class of the phase transition.

III. HOMOGENEOUS SYSTEMS

A. Two dimensions

Our results for the two-dimensional phase diagram in Fig. 1 are based on the fact that the model in Eq. (1) undergoes a BKT transition as a function of the temperature. This phase transition has been studied in great detail the context of the two-dimensional quantum XY model in Eq. (2) in the absence of a magnetic field [60–63]. Kosterlitz and Thouless predicted that the superfluid stiffness ρ_s jumps from zero to the value $(2/\pi)T_c$ at the critical temperature. Thus we consider measurements of the superfluid stiffness ρ_s for different system sizes L as a function of temperature. Within the SSE method, the superfluid stiffness is computed by measuring the
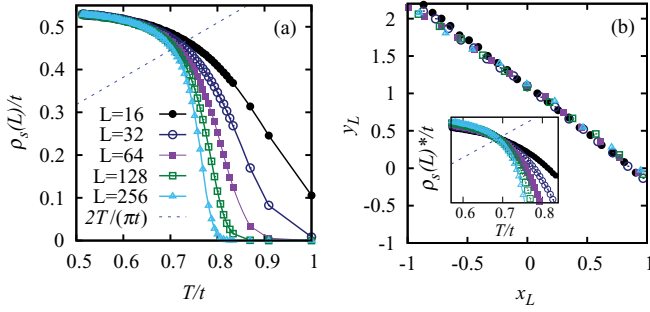
FIG. 2. (Color online) (a) Superfluid stiffness in 2D for $\mu = 0$ and several values of L. The error bars (not shown) are smaller than the point size used in the plot. (b) Data collapse according to the relation in Eq. (4). The inset in (b) shows the rescaled superfluid stiffness vs T.

fluctuations of the winding number W [64]; they are connected through the relation $\rho_s = \langle W^2 \rangle / 2\beta$, where $\beta = 1/T$ is the inverse temperature.

Figure 2(a) shows results for the superfluid stiffness of 2D hard-core bosons at $\mu = 0$ [or, equivalently, the spin stiffness of the 2D XY model in Eq. (2)] as a function of T for several system sizes. The observed slow approach of the superfluid stiffness to the characteristic jump expected for the infinite system is due to strong finite-size effects at the BKT transition. Finite-size scaling relations for the superfluid stiffness can be derived by integrating the Kosterlitz renormalization-group equations (see, for instance, Refs. [63,65,66]). This procedure yields

$$\frac{\rho_s(T,L)\pi}{2T} - 1 = c \coth 2c \left(\ln L + l_0 \right), \quad T < T_c,$$

$$\frac{\rho_s(T_c,L)\pi}{2T} - 1 = \frac{1}{2 \left(\ln L + l_0 \right)}, \qquad T = T_c, \qquad (3)$$

$$\frac{\rho_s(T,L)\pi}{2T} - 1 = c \cot 2c \left(\ln L + l_0 \right), \quad T > T_c,$$

where c measures the distance from the critical point and l_0 depends only weakly on temperature. Close to the critical point, $c \sim \sqrt{|T - T_c|}$. In the limit $2c (\ln L + l_0) \ll 1$, a scaling form for the superfluid stiffness based on Eq. (3) can be written as

$$\frac{\rho_s(T,L)\pi}{T} - 2 = \frac{1}{\ln L + l_0} F[(\ln L + l_0)^2 (T - T_c)]. \quad (4)$$

From Eq. (3) in the limit $2c (\ln L + l_0) \ll 1$, $F(x) = 1 - (4/3)x$. From Eq. (4), one can find the scaling function F and critical temperature T_c by computing $x_L = (\ln L + l_0)^2 (T - T_c)/t$ and $y_L = \rho_s(T,L)\pi/T - 2$ based on our Monte Carlo simulations for different L and T. The adjustment of the constant l_0 and critical temperature T_c, such that the data produce the best possible collapse, yields a numerical estimate of the scaling function F and the critical temperature itself. The result of the determination of the scaling function F is reported in Fig. 2(b), where a plot of y_L as a function of x_L is presented. Notice that, as expected, the value of F is very close to one for $x_L = 0$. Furthermore, one expects from Eq. (3) that a plot of the rescaled superfluid stiffness $\rho_s(T,L)^* = \rho_s(T,L)(1 + \frac{1}{2[\ln L + l_0]})^{-1}$ as a function of the temperature T should become system-size independent

at the critical temperature T_c. This observation is confirmed in the inset of Fig. 2(b). Remarkably, those curves intersect with the line $(2/\pi)T$ right at the critical temperature, in agreement with the BKT scenario. Our result $T_c/t = 0.685 \pm 0.001$ is consistent with the best value reported in Ref. [63], for which $T_c/t = 0.6846 \pm 0.0006$ [67]. An analogous procedure to the one just described is carried out for different values of the chemical potential to complete the two-dimensional phase diagram in Fig. 1. We should mention that Eq. (3) predicts the value of the superfluid stiffness in an infinite system at the critical temperature to be $\rho_s(T_c)/T_c = 2/\pi$. However, in Ref. [68], it was shown that the superfluid stiffness at the transition temperature is $\rho_s(T_c)/T_c \simeq 0.63650$, which is very close to the result based on Eq. (3) ($2/\pi \simeq 0.63662$). Detecting the difference is beyond the accuracy of the present study.

1. Critical value from dn_0/dT

We now briefly discuss the behavior of the occupation of the zero-momentum state ($n_{k=0} \equiv n_0$) in the critical region and address the determination of the transition temperature from it. In a homogeneous and infinite 3D system, BEC is identified by a macroscopic occupation of n_0. However, as mentioned before, thermal fluctuations in 2D destroy Bose-Einstein condensation. Nonetheless, as the superfluid transition is approached from the normal phase, n_0 diverges [see inset in Fig. 3(a)]. Indeed, from the Fourier transform of the one-body density matrix in the long-distance limit $\langle \hat{a}_i^\dagger \hat{a}_{i+r} \rangle \propto r^{-1/4} \exp(-r/\xi)$, one can extract the behavior of n_0 as T_c is approached,

$$n_0 \sim \xi^{7/4}. \quad (5)$$

We assume the essential singularity of the correlation length $\xi \sim e^{b/\sqrt{T - T_c}}$, where b is a chemical-potential-dependent scaling factor. From Eq. (5), it follows that not only does n_0 diverge at T_c, but also its derivative with respect to T,

$$\frac{dn_0}{dT} \sim -\frac{\xi^{7/4} \ln^3 \xi}{b^2}. \quad (6)$$

In a finite system, when T is close to T_c, the role of the correlation length is taken over by L when $\xi \gtrsim L$. This occurs
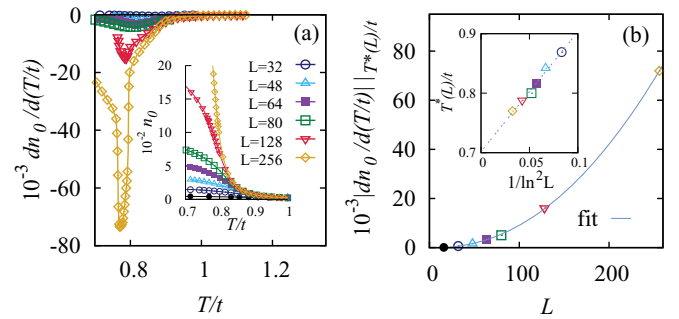
FIG. 3. (Color online) (a) Derivative of the zero-momentum occupation n_0 with respect to the temperature for different values of L. The inset shows n_0 vs T. (b) Finite-size scaling of the height of the negative peak in dn_0/dT. The continuous line is a fit to the function $g(L) = a_0 + a_1 L^{7/4} \ln^3(a_2 L)$. The inset shows the finite-size scaling of $T^*(L)$.

at a characteristic temperature $T^*(L)$ given by

$$T^*(L) = T_c + b'/\ln^2 L, \quad (7)$$

where b' is a nonuniversal factor related to b. At that temperature, the derivative in Eq. (6) scales with the system size as

$$\left.\frac{dn_0}{dT}\right|_{T^*(L)} \sim -\frac{L^{7/4}\ln^3 L}{b^2}. \quad (8)$$

Below $T^*(L)$, n_0 cannot vary as fast as right above $T^*(L)$ because the exponential increase of the correlation length is truncated by L. Below $T^*(L)$, the variation of n_0 comes mainly from the temperature dependence of the anomalous exponent, which is not as strong as the variation due to the exponential behavior of the correlation length. Consequently, dn_0/dT should exhibit a sharp minimum at the size-dependent temperature $T^*(L)$. Moreover, in a finite system, n_0 cannot grow indefinitely as the temperature is lowered. With decreasing temperature ($T \to 0$), n_0 must approach its (finite) $T = 0$ value, which implies that $dn_0/dT \to 0$.

Figure 3(a) depicts the derivative of the n_0 for different system sizes vs T. The divergence of dn_0/dT is apparent. A sharp minimum develops and its location $T^*(L)$ approaches T_c as the system size increases. This is expected from the finite-size relation in Eq. (7). The scaling of the height of this minimum is studied in Fig. 3(b), where we plot the absolute value of $dn_0/dT|_{T^*(L)}$ vs L. The data follows the scaling relation in Eq. (8), as made evident by a fit to the function $g(L) = a_0 + a_1 L^{7/4}\ln^3(a_2 L)$. In the inset in Fig. 3(b), we show the finite-size scaling of $T^*(L)$. We observe that $T^*(L)$ is consistent with the scaling relation in Eq. (7), which we use to obtain the critical temperature in the thermodynamic limit. We find $T_c/t = 0.701 \pm 0.007$. This value is compatible with the one found by performing the finite-size scaling of the superfluid stiffness. While this approach is obviously less accurate than the one discussed before for ρ_s, among other things because a numerical derivative is involved, the fact that it works extremely well is very important for current trapped ultracold gas experiments where the superfluid density cannot be measured.

We note at this point that in the determination of Eq. (8), we have neglected multiplicative logarithmic corrections that affect the behavior of the zero-momentum occupation and thus its derivative with respect to the temperature [69,70]. In fact, the exponent of the logarithm in Eq. (8) gets modified to

$$\left.\frac{dn_0}{dT}\right|_{T^*(L)} \sim -\frac{L^{7/4}\ln^{3-2r} L}{b^2}, \quad (9)$$

with $r = -1/16$ (Ref. [70]). However, this correction does not affect the determination of the critical temperature, which is based on the location of the position of the peak in the numerical derivative and the scaling relation in Eq. (7). Furthermore, the correction to the exponent of the logarithm is very small and, at least within the precision of our simulations, its effect is hardly detectable.

B. Three dimensions

In order to determine the 3D phase diagram, we follow the same procedure as in 2D. In 3D, however, the superfluid to

normal transition belongs to the 3D XY universality class. This transition, for the model in Eq. (1), has also been studied using QMC simulations in the past. T_c for BEC was evaluated as a function of the density in Ref. [71]. The onset of magnetization as a function of the magnetic field (or, in the bosonic language, the density as a function of the chemical potential) was investigated in Ref. [72]. Furthermore, the fate of the superfluid phase under the effect of an additional ring-exchange term was studied in Ref. [73]. Here, we determine the full phase diagram (shown in Fig. 1) as a function of the temperature and the chemical potential. We begin by considering measurements of the superfluid stiffness. In $d > 2$ dimensions, as the critical temperature is approached, the superfluid stiffness vanishes continuously as [74]

$$\rho_s \sim |T_c - T|^{(d-2)\nu}, \quad (10)$$

where the exponent ν determines how the correlation length diverges when approaching the critical temperature, i.e.,

$$\xi \sim |T - T_c|^{-\nu}. \quad (11)$$

As a result, at the critical temperature, the superfluid stiffness scales with the linear size of the system as $\rho_s \sim L^{2-d}$. This, in turn, allows one to write the scaling hypothesis for the superfluid stiffness as a function of the system size and the temperature as

$$\rho_s L^{d-2} = F(|T - T_c|L^{1/\nu}), \quad (12)$$

which we utilize to determine the critical temperature. In Fig. 4(a), we show results for the superfluid stiffness in a 3D lattice vs T for different system sizes.

We numerically extract the scaling function F by studying the rescaled superfluid stiffness [left-hand side in Eq. (12)] vs the rescaled temperature $(T - T_c)L^{1/\nu}$. Classical Monte Carlo simulations yield the correlation length exponent $\nu = 0.6717 \pm 0.0001$ [52], and $\nu = 0.6717 \pm 0.0003$ [53], which we use to produce the collapse presented in Fig. 4(b). With ν at hand, it is enough to fix T_c such that the best collapse of the data is achieved. Furthermore, the inset shows the rescaled superfluid stiffness as a function of temperature, which becomes system-size independent at the critical temperature, as implied by the scaling hypothesis in Eq. (12). Our best estimation of the critical temperature for $\mu = 0$ is $T_c/t = 2.0169 \pm 0.0005$ (to be compared with $T_c/t = 1.94$ from Ref. [71] and more recently with $T_c/t = 2.016 \pm 0.004$ from
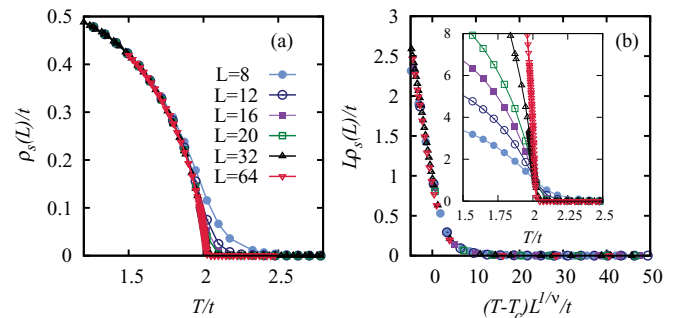
FIG. 4. (Color online) (a) Superfluid stiffness of the 3D system for $\mu = 0$ and several values of L. (b) Data collapse according to the relation in Eq. (12). The inset shows the rescaled superfluid stiffness as a function of T.
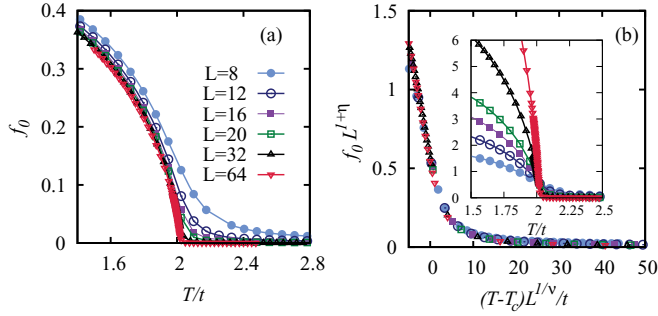
FIG. 5. (Color online) (a) Condensate fraction in 3D for $\mu = 0$ and several values of L. (b) Data collapse according to the relation in Eq. (14). The inset shows the rescaled condensate fraction as a function of T.

Ref. [75]). We perform a similar analysis for different values of the chemical potential to complete the three-dimensional phase diagram in Fig. 1.

Additionally, since the superfluid to normal phase transition in our model in 3D is accompanied by the emergence of true long-range order, one can study the transition by computing the condensate fraction f_0 associated with the appearance of BEC. Following Penrose and Onsager [76], the condensate fraction is defined as the ratio of the largest eigenvalue of the one-body density matrix to the total number of particles N_b. For the system under consideration, condensation occurs to the zero-momentum state due to translational invariance, thus the condensate fraction is $f_0 = n_0/N_b$. The behavior of n_0 can be obtained from the Fourier transform of the one-body density matrix in the long-distance limit, which in 3D is given by

$$\langle \hat{a}_i^\dagger \hat{a}_{i+r} \rangle \propto r^{-(1+\eta)} \exp\left(-r/\xi\right). \tag{13}$$

Here, η is the correlation function exponent, also known as the anomalous scaling dimension. On approach to T_c, n_0 diverges with the correlation length as [29]

$$n_0 \sim \xi^{2-\eta}. \tag{14}$$

In a finite system, this relation implies that the condensate fraction vanishes at the critical point as $f_0 \sim L^{-(1+\eta)}$, which we adopt to formulate the following scaling hypothesis for the condensate fraction:

$$f_0 L^{1+\eta} = F(|T - T_c| L^{1/\nu}). \tag{15}$$

In the determination of T_c through the scaling relation in Eq. (15), we use the value $\eta = 0.0381 \pm 0.0002$ [52]. The results are summarized in Fig. 5, where a plot of the condensate fraction vs T is shown in panel (a). In Fig. 5(b), the data collapse of the rescaled condensate fraction $f_0 L^{1+\eta}$ vs the rescaled temperature is apparent. Furthermore, in the inset, one can observe that curves of the rescaled condensate fraction vs T become system-size independent at T_c, as implied in Eq. (15). This procedure results in a $T_c/t = 2.0167 \pm 0.0005$ for $\mu = 0$, which is in remarkably good agreement with our previous estimate using the superfluid stiffness.

1. Critical value from dn_0/dT

Similarly to the 2D case, dn_0/dT diverges in the vicinity of the superfluid to normal phase transition. It diverges with

the correlation length as

$$\frac{dn_0}{dT} \sim -\xi^{2-\eta+1/\nu}. \tag{16}$$

Also, as in 2D, in a finite 3D system at a temperature $T^*(L)$ close to T_c, the role of the correlation length is taken over by L when $\xi \gtrsim L$. The characteristic temperature $T^*(L)$ is given by

$$T^*(L) = T_c + c'/L^{1/\nu}, \tag{17}$$

where c' is a nonuniversal factor. At $T^*(L)$, dn_0/dT scales with the system size as

$$\left.\frac{dn_0}{dT}\right|_{T^*(L)} \sim -L^{2-\eta+1/\nu}. \tag{18}$$

Furthermore, in a finite system, dn_0/dT reaches its minimum value at $T = T^*(L)$ because the divergence of the correlation length can no longer be sustained. This is expected from the behavior of n_0 vs T, shown in the inset in Fig. 6(a), where n_0 is first seen to increase as the temperature is lowered and then to saturate as $T \to 0$. The changes observed, dn_0/dT, in that low-temperature regime originate in the smooth dependence of the correlation function exponent on the temperature, as opposed to the fast change produced by the strong divergence of the correlation length. Hence, once again, dn_0/dT exhibits a sharp minimum at the size-dependent temperature $T^*(L)$ in Eq. (17) and then goes to zero.

In Fig. 6(a), we display results for dn_0/dT vs T for different system sizes. The divergence in the derivative, anticipated by Eqs. (16) and (18), is confirmed by the presence of sharp minima that grow with system size. The finite-size scaling of the height of the sharp minimum in Eq. (18) is presented in Fig. 6(b), where we plot the logarithm of the maximum height of $|dn_0/dT|$ vs $\ln L$. According to Eq. (18), such a plot should turn into a straight line with a slope given by $m = 2 - \eta + 1/\nu$. A fit of our data to the function $g(\ln L) = a_0 + a_1 \ln L$ yields $a_1 = 3.47 \pm 0.01$. The scaling relation given by Eq. (18) is thus confirmed as our value of a_1 is compatible with the exponents from Ref. [52], which yield $m = 3.450$. The size dependence of the position of the peaks anticipated in Eq. (17) is verified in the inset of Fig. 6(b). Within this procedure, we find that the critical temperature in the thermodynamic limit is $T_c/t = 2.012 \pm 0.002$, which is in relatively good agreement with
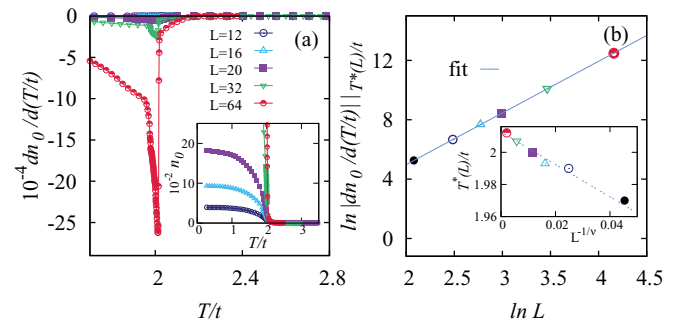
FIG. 6. (Color online) (a) dn_0/dT for different values of L. The inset shows n_0 vs T. (b) Finite-size scaling of the height of the negative peak in dn_0/dT. The continuous line is a fit to the function $g(\ln L) = a_0 + a_1 \ln L$. The inset shows the finite-size scaling of $T^*(L)$.

the one obtained through the finite-size scaling of both the superfluid stiffness and the condensate fraction.

We conclude this section by mentioning that in determining the critical temperature, we have used the leading scaling forms and subleading corrections to scaling have been neglected. For the 3D XY universality class, such corrections have been reviewed in Ref. [77]. We note that in our calculations, there is an excellent collapse of the data, which suggests that the effects of the subleading corrections to scaling are small. Furthermore, the most accurate results obtained for T_c follow from completely independent measurements, i.e., the superfluid and condensate fractions. They agree within the error bars, which further supports the relevance of the scaling relations used.

C. Mean field

To gain an understanding of the effects of quantum fluctuations in our systems, we have also calculated the mean-field phase diagram for this model. We utilize the standard decoupling of the kinetic energy term in the Hamiltonian in Eq. (1) [78],

$$\hat{a}_i^\dagger \hat{a}_j \simeq \hat{a}_i^\dagger \Phi_j + \hat{a}_j \Phi_i^* - \Phi_i^* \Phi_j, \qquad (19)$$

where $\Phi_i = \langle \hat{a}_i \rangle$ is the condensate order parameter, to be determined self-consistently. The angle brackets denote the usual thermal average. The above mean-field decoupling allows one to write a mean-field Hamiltonian for Eq. (1) as

$$\hat{\mathcal{H}}_{\text{MF}} = -t \sum_{\langle i,j \rangle} (\hat{a}_i^\dagger \Phi_j + \Phi_i^* \hat{a}_j - \Phi_i^* \Phi_j) + \text{H.c.} - \sum_i \mu_i \hat{n}_i. \tag{20}$$

For homogeneous systems, i.e., $V_0 = 0$, Eq. (20) can be recast in the following manner:

$$\hat{h}_{\text{MF}} = -2dt\,\Phi(\hat{a}^\dagger + \hat{a}) - \mu \hat{n}, \qquad (21)$$

where $\hat{h}_{\text{MF}}$ is the mean-field Hamiltonian per lattice site. Note that in this case, the superfluid order parameter can be taken to be real. The corresponding partition function at finite inverse temperature β is

$$Z = 2e^{-\beta \frac{\mu}{2}} \cosh \beta \sqrt{\frac{\mu^2}{4} + (2dt\,\Phi)^2}. \qquad (22)$$

A self-consistency condition for the superfluid order parameter can be derived by noting that

$$\frac{dZ}{d\Phi} = 4\beta dt \langle \hat{a} \rangle Z. \qquad (23)$$

Using the relation (23), we arrive at the equation that determines the order parameter Φ,

$$\sqrt{\frac{\mu^2}{4} + (2dt\,\Phi)^2} = dt \tanh \beta \sqrt{\frac{\mu^2}{4} + (2dt\,\Phi)^2}, \qquad (24)$$

which is valid whenever $\Phi > 0$. We solve Eq. (24) numerically and determine the superfluid region, $\Phi > 0$, as a function of the temperature and the chemical potential. The phase boundaries are determined as the values of μ and T for which $\Phi \to 0$. For $\mu = 0$, Eq. (24) reduces to

$$2\Phi = \tanh \beta\, 2dt\,\Phi, \qquad (25)$$

which is the equation that determines the mean-field magnetization of the Ising model in the absence of a magnetic field. The critical temperature is, of course, $T_c/td = 1$, which is quite different from the results of our quantum Monte Carlo simulations in two and three dimensions.

IV. TRAPPED SYSTEMS

In experiments involving ultracold atoms, an additional trapping potential is necessary to contain the gas. While a qualitative (and sometimes a reasonably good quantitative) description of the trapped system can be obtained within the local density approximation (LDA) from the properties of the homogeneous system, this approximation may break down in regimes of interest. In particular, the latter occurs at criticality, where the correlation length diverges and deviations from the LDA description can be large [29]. Furthermore, as we explain below, in trapped 2D systems care needs to be taken with the application of the Mermin-Wagner-Hohenberg theorem. Therefore, we focus our attention on those two aspects, namely, the possibility to have BEC in the presence of an additional external confining potential in 2D, and the study of criticality in 2D and 3D.

A. Absence of BEC in interacting 2D systems

We mentioned in Sec. I that homogeneous 2D systems are special because thermal fluctuations destroy any order at finite temperature. However, harmonically confined noninteracting bosons can undergo BEC at finite temperature [79]. In this case, the arguments by Mermin *et al.* are not violated because condensation does not occur to the zero-momentum state, but to a single-particle eigenstate of the trapped system. One can then wonder whether finite-temperature BEC persists in the presence of interactions. By following analogous arguments to those in Ref. [80], we show below that interactions do preclude the formation of a condensate in the Bose-Hubbard model in the presence of the trap. This is so because there is a close connection between the formation of a condensate and the macroscopic population of the zero-momentum occupation, which is forbidden in 2D at finite temperature.

Generally speaking, the emergence of BEC is established through the evaluation of the condensate fraction f_0, which is defined as the ratio of the largest eigenvalue of the one-body density matrix n_M to the total number of particles N_b,

$$f_0 = \frac{n_M}{N_b}. \qquad (26)$$

If after taking the appropriate thermodynamic limit f_0 remains finite, then the system exhibits BEC. Otherwise, if it becomes zero, there is no condensation [76].

Alternative forms of the criteria expressed through Eq. (26) can be useful when the system is not spatially uniform; they are based on the following inequality [76]:

$$n_M^2 \leqslant \sum_a n_a^2 \leqslant n_M \sum_a n_a = n_M N_b, \qquad (27)$$

where n_a are the eigenvalues of the one-body density matrix ρ_{ij}. We define the quantity

$$A_2 = N_b^{-2} \sum_{i,j} |\rho_{ij}|^2, \tag{28}$$

which is just a lattice version of its analogous quantity defined on the continuum in Ref. [76]. It follows from Eqs. (27) and (28) that

$$f_0^2 \leqslant A_2 \leqslant f_0. \tag{29}$$

Therefore, if A_2 remains finite in the thermodynamic limit, then the system exhibits BEC. A further criterion can be defined and it depends on the quantity

$$A_1 = (N_b L^d)^{-1} \sum_{i,j} |\rho_{ij}|. \tag{30}$$

Notice that $(A_1 N_b / L^d)^2$ is the square of the mean value of the function $|\rho_{ij}|$, while $A_2 (N_b / L^d)^2$ is the mean value of $|\rho_{ij}|^2$. Since the variance of the function $|\rho_{ij}|$ is either positive or zero, it follows that

$$A_1^2 \leqslant A_2. \tag{31}$$

Now, since ρ_{ij} is a positive-semidefinite Hermitian matrix, its elements satisfy [76,81]

$$|\rho_{ij}| \leqslant \sqrt{\rho_{ii}\, \rho_{jj}} \leqslant \tfrac{1}{2}(\rho_{ii} + \rho_{jj}) \leqslant \alpha N_b / L^d, \tag{32}$$

where $\alpha N_b / L^d$ is an upper bound of the local density ρ_{ii}. By summing over i and j in Eq. (32) and the square of it, we find a lower bound for A_1,

$$A_2 \leqslant \alpha A_1. \tag{33}$$

As long as the local density ρ_{ii} remains finite throughout the whole system, α can be taken to be finite and independent of N_b / L^d. This, in turn, implies that if $A_1 > 0$, then BEC takes place; otherwise if $A_1 = 0$, then no BEC occurs [76]. Notice that if $\rho_{ij} \geqslant 0$, then A_1 coincides with the ratio of the zero-momentum occupation to the total number of particles, i.e., the fraction of particles in the system that condenses to the zero-momentum state. Since in two dimensions n_0 / N_b vanishes because of the Mermin *et al.* theorem, A_1 is zero too. In the specific case of the Bose-Hubbard model in the presence of an inhomogeneous potential in thermal equilibrium, we have that $\rho_{ij} \geqslant 0$. Furthermore, the density is finite everywhere across the system because of the on-site interaction, implying that $A_1 = 0$.

Hence, even in the presence of the trap, there is no condensation in the 2D Bose-Hubbard model at finite T. Note that this argument does not preclude condensation in the noninteracting limit, where the density can diverge at the minimum of the inhomogeneous potential in the thermodynamic limit and BEC can indeed occur to the lowest single-particle eigenstate, but not to the zero-momentum state. Moreover, the criteria above implies that for the Bose-Hubbard model in $d > 2$ in thermal equilibrium, condensation to any state has to be accompanied by condensation to the zero-momentum state.

In our proof, we have stated that for the Bose-Hubbard model in thermal equilibrium, $\rho_{ij} \geqslant 0$ holds. We now present two independent arguments for why $\rho_{ij} \geqslant 0$. The first one is based on the fact that the matrix elements of the von

Neumann's statistical operator in the position representation are strictly positive [82]. Since the one-body density matrix corresponds to a partial trace of the von Neumann's statistical operator [76], it follows that its elements are positive too. A rather technical, but yet rigorous, argument is based on the series-expansion representation of the one-body density matrix that we used in our Monte Carlo implementation. Within this representation, the measurements of the one-body density matrix are based on the extension of the configuration space where these off-diagonal quantities are well defined [59]. In such extended space, the one-body density matrix is represented as the sum of strictly positive matrix elements (hence $\rho_{ij} \geqslant 0$), which are, in turn, efficiently sampled during the construction of the loop operators in the directed-loop update algorithm [83].

B. Two dimensions

1. Local compressibility

Exactly as in the homogeneous system, even though there is no condensation in 2D, a superfluid phase is expected in the trapped system at low temperatures. Because of the inhomogeneity introduced by the confining potential, the coexistence of space separated normal and superfluid domains can occur at intermediate temperature. In that case, there must be a region in the trap where superfluidlike domains transition into normal ones. Within the LDA, this region is such that the local chemical potential μ_i coincides with the critical μ of the bulk system for the normal to superfluid phase transition.

Based on this idea, Zhou and collaborators proposed a method to identify the phase boundaries of the homogeneous system from a high-resolution scan of the local density $\rho(r)$ across the confined system [31]. This method requires the determination of the local compressibility defined as

$$\kappa_{\text{diff}}(r) = -\frac{1}{2V_0 r} \frac{d\rho(r)}{dr}, \tag{34}$$

and relies on the expectation that the local density profile $\rho(r)$, as well as the local compressibility $\kappa_{\text{diff}}(r)$, can be well approximated by their bulk values through the LDA. The existence of sharp features in the local compressibility at specific locations in the trap is then associated with phase transitions occurring in the homogeneous system as a function of the chemical potential. This method is expected to be accurate in the limit of very shallow traps where the contribution from density gradients due to the trapping potential are small [84].

In Fig. 7, we present QMC results for the density profile of a 2D trapped system, as well as the local compressibility, as a function of the distance from the center of the trap. The expected sharp features in the local compressibility due to critical fluctuations are smoothed by finite-size effects. They are replaced by a rounded maximum, which can be associated with the superfluid to normal transition [84]. The location of the maximum r_c is connected to the critical chemical potential through $\mu_c = \mu - V_0 r_c^2$. For the case in Fig. 7, we get $\mu_c / t = -3.57 \pm 0.03$. This value is to be contrasted with $\mu_c / t = -3.5$, which we obtained in the homogeneous system calculations. As T increases, however, the agreement between
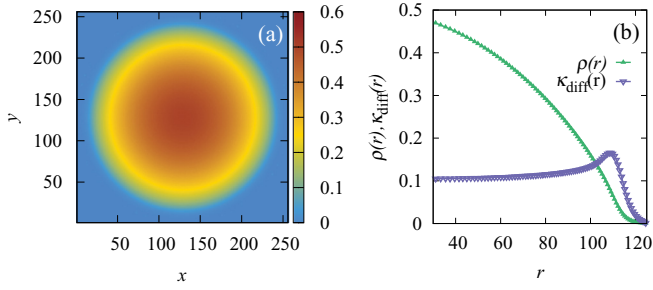
FIG. 7. (Color online) (a) Two-dimensional density at $T/t = 0.2012$ and a trapping potential $V_0/t = 0.0003$, for $\mu = 0$ in the center of the trap. (b) The corresponding density profile $\rho(r)$, as well as the local compressibility $\kappa_{\text{diff}}(r)$, as a function of the distance from the center of the trap r. All distances x, y, and r are measured in units of a, while the local compressibility is measured in units of $1/t$.

FIG. 8. (Color online) (a) n_0 as a function of T and β in a trapped 2D system with $V_0/t = 0.00125$, $\mu = 0$ in the center of the trap, and $L = 128$. (b) Derivatives of n_0 with respect to β and with respect to T.

the estimates of the critical chemical potential based on the local compressibility and the results of the homogeneous system worsens. For instance, for $T/t = 0.4562$, we find that $\mu_c/t = 2.99 \pm 0.04$, as opposed to the homogeneous system result where $\mu_c/t = 2.5$. This occurs presumably because closer to the tip of the superfluid lobe, critical fluctuations are stronger, and thus larger violations of the LDA are expected.

2. Momentum distribution function

Another quantity that can be measured in experiments with ultracold atoms is the momentum distribution function. At fixed chemical potential ($\mu \leqslant 0$), when lowering T, the normal to superfluid crossover in the trapped system proceeds via the creation and growth of a superfluid domain in the center of the trap. (The rate of growth of the superfluid domain will depend on the functional form and strength of the confining potential.) Hence, the zero-momentum state becomes increasingly populated. As follows from the discussion for finite homogeneous systems, it is expected that as T decreases and approaches T_c for the normal to superfluid transition in the center of the trap, the rate of growth of n_0 will increase. Below T_c, on the other hand, dn_0/dT will eventually decrease because of the finite extend of the system imposed by the confining potential. If T is lowered well below T_c, then almost the entire system will become superfluid and the observables will saturate their (finite) zero-temperature values.

Hence, just as in the homogeneous case, one can attempt to estimate T_c for the superfluid to normal phase transition for the density in the center of the trap by measuring the temperature at which the rate of change of n_0 is extremal. This approach provides an accurate estimate for the homogeneous system and it is expected to be accurate in confined systems with shallow trapping potentials. Figure 8(a) depicts the evolution of n_0 vs T as well as the inverse temperature β of a harmonically confined 2D system with $V_0/t = 0.0015$ ($L = 128$) and $\mu = 0$ in the center of the trap. In Fig. 8(b), we show dn_0/dT which, as expected, exhibits a minimum located at $T/t = 0.66 \pm 0.02$. This temperature is compatible with the value of T_c/t obtained for the homogeneous case where, after a finite-size scaling, we obtained $T_c/t = 0.685 \pm 0.001$. Our estimate derived from the
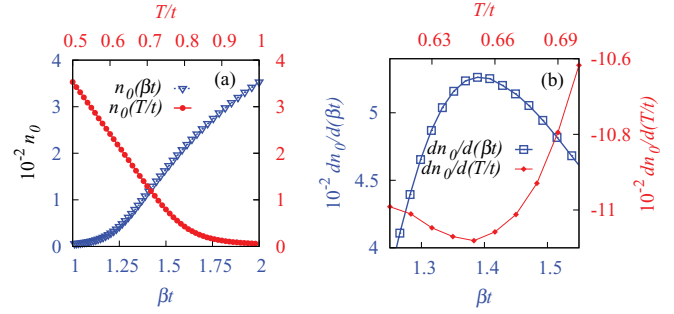
study of a single trapped system is about 4% off the value of the homogeneous system.

One can perform the same analysis based on measurements of n_0, but now as a function of the inverse temperature β. In that case, one expects a maximum in the derivative $dn_0/d\beta$ instead of a minimum. In general, for finite and not very large systems, the position of such maximum β_c will not coincide with $1/T_c$ obtained from the minimum of dn_0/dT. Overall, we find that for the system sizes available to our QMC simulations, the analysis based on $dn_0/d\beta$ provides more accurate estimates of the critical temperature than the one based on dn_0/dT. Furthermore, the maximum found in $dn_0/d\beta$ is consistently sharper and better defined with respect to the minimum found for dn_0/dT, which instead is shallower and broader, and thus harder to detect and numerically less reliable.

Based on measurements of $dn_0/d\beta$ presented in Fig. 8(b) on the same system with $V_0/t = 0.0015$ ($L = 128$), $\mu = 0$, we find $T_c/t = 0.72 \pm 0.02$, which is also very close to the critical temperature of the homogeneous system. When the maximum is sharply defined, in the limit of very shallow traps with large numbers of bosons, the two approaches are expected to coincide (i.e., their difference is due to finite-size effects). As a matter of fact, for the homogeneous 2D and 3D systems in Sec. III, where the minima of dn_0/dT are sharp, we find that the analysis using dn_0/dT and $dn_0/d\beta$ yields essentially the same results for T_c. In the Appendix, we provide an analytic understanding of this in terms of a simple function. Therefore, for the determination of the phase diagram based on measurements in harmonically confined systems, we consider only measurements based on $dn_0/d\beta$.

In Fig. 9, we summarize our results for the determination of the critical parameters with the local compressibility as well as with the derivative of the zero-momentum occupation with respect to β, and contrast them with the phase diagram of the homogeneous system. Clearly, all methods work well for large values of μ/t and small values of T_c/t (equivalent to approaching the continuum limit in a lattice system). Close to the tip of the superfluid region, the method based on n_0 performs much better than the one based on $\kappa_{\text{diff}}(r)$.

At the tip of the superfluid lobe, where the size effects are expected to be the strongest, we observe that as the size of the system is increased (or the strength of the trap is decreased), keeping constant the chemical potential in the
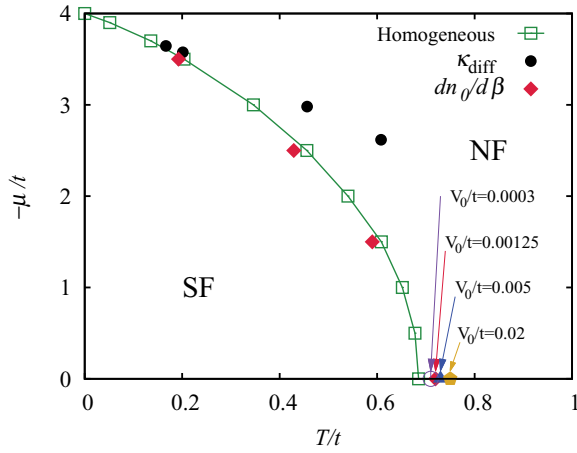
FIG. 9. (Color online) Estimate of the critical points based on the local compressibility (black dots; based on a system with $L = 256$) as well as the derivative of the zero-momentum occupation with respect to β (red diamonds; based on a system with $L = 128$). At the tip of the superfluid lobe, we include further results for different system sizes and trap strengths (yellow pentagon: $L = 32$; blue triangle: $L = 64$; violet empty circle: $L = 256$). The phase diagram of the homogeneous system is also shown.

center of the trap, the estimate of the critical temperature decreases, approaching the result in homogeneous systems.

C. Three dimensions

We now turn our attention to the study of criticality in 3D trapped systems. We make use of the same ideas developed for 2D system to extract the critical parameters, i.e., measurements based on the zero-momentum occupation as well as on the local compressibility.

Additionally, in 3D, we can utilize a method that is based on the analysis of the shape of the central peak for the momentum distribution. With it, one can construct a quantity that exhibits a minimum at the critical point [29]. The idea behind this method is that close to criticality, the momentum distribution develops a bimodal structure whose evolution as a function of temperature contains information about the formation of a superfluid region in the center of the trap. At T_c, when a superfluid domain begins to form, the major contribution to the occupation of the zero-momentum state comes from regions that are not critical, i.e., from regions that are far away from the center of the trap. However, the derivatives of the momentum distribution $d^m n_k / dk^m$ are critical, in the sense that they can be understood in terms of an LDA integral that diverges at the center of the trap, where the system is critical. Based on that idea, the following quantity was devised in order to extract the critical temperature [29]:

$$Q(T) = (n_0 - n_{k_{\max}})(k_{\max})^s, \qquad (35)$$

where $k_{\max}$ is the momentum at which $|dn_k / dk|$ is maximum and the exponent $s > 2 - \eta$. In Ref. [29], it was shown that $Q(T)$ should exhibit a minimum at the critical temperature T_c.

We plot $Q(T)$ vs T in Fig. 10(a). $Q(T)$ exhibits a minimum at $T_c / t = 2.04 \pm 0.03$. In the inset, we show the evolution of the momentum distribution function as the temperature
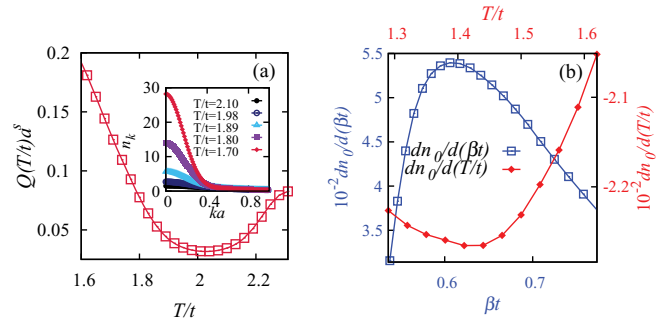
FIG. 10. (Color online) (a) The quantity $Q(T)$ as a function of temperature extracted from the momentum distributions shown in the inset. The exponent in Eq. (35) has been set to $s = 3$. (b) Derivatives of n_0 with respect to β and with respect to T. The three-dimensional system is prepared with $V_0 / t = 0.04$, $\mu = 0$, and $L = 32$.

of the system is reduced. This result is compatible with the critical temperature found for the homogeneous system $T_c / t = 2.0169 \pm 0.0005$. In principle, similar ideas to the ones presented in Ref. [29] could be used to devise a quantity $Q(T)$ to locate the critical parameters in 2D. In that case, however, the structure of the momentum distribution is different because the transition is in another universality class. As a result, the LDA integrals for the central peak and the derivatives of the momentum distribution get substantially modified. We find that both the central peak and the derivatives of n_k are critical in 2D because the LDA integrals of those quantities diverge in the center of the trap where the system is critical. Hence, one cannot define a $Q(T)$, as done in 3D, that will exhibit a minimum at T_c.

In Fig. 10(b), we also display results obtained for $dn_0 / d\beta$ (dn_0 / dT) in the same system. The temperature at which the maximum (minimum) occurs for those quantities exhibits a larger deviation from T_c, from the homogeneous case, than $Q(T)$. However, with increasing system size, we find that the maxima of $dn_0 / d\beta$ (minima of dn_0 / dT) slowly approach the homogeneous result. In experiments where the system sizes are much larger than the ones studies here, we expect that dn_0 / dT and $dn_0 / d\beta$ will both produce accurate results for T_c.

In Fig. 11, we present a summary of our estimates of the critical parameters based on the local compressibility, the derivatives of n_0 with respect to β, and Eq. (35). The method based on $Q(T)$ is found to be more accurate than those based on $dn_0 / d\beta$ and the local compressibility. This is understandable because the former approach uses precise information of the nature and universality class of the transition in 3D. Nevertheless, as argued before, we anticipate that if one decreases the strength of the confining potential and increases the number of bosons, as to reach the system sizes that are studied experimentally, then $dn_0 / d\beta$ will provide accurate results (at least similar to the ones obtained in 2D). This effect is studied in Fig. 11 where we show the evolution of the critical temperature at the tip of the lobe as a function of system size. As the strength of the confining potential is decreased and the size of the system is increased, the estimate of the critical temperature based on $dn_0 / d\beta$ tends to increase and approach T_c in the homogeneous system. The method based on the local compressibility is found to be inadequate
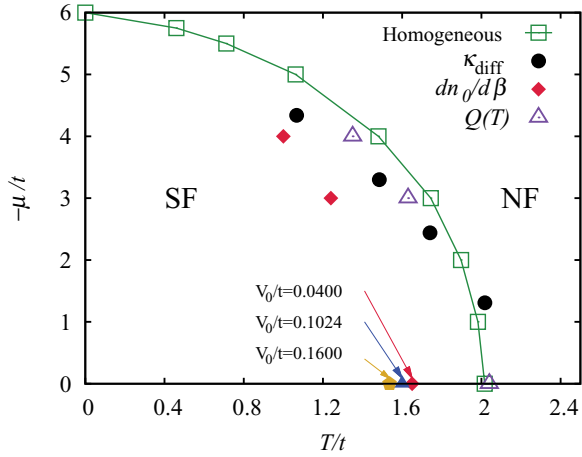
FIG. 11. (Color online) Estimates of the critical points based on the local compressibility (black dots; based on a system with $L = 64$) as well as the derivatives of the zero-momentum occupation with respect to β (red diamonds; based on a system with $L = 32$). At the tip of the superfluid lobe, we include further results for different system sizes and trap strengths (yellow pentagon: $L = 16$; blue triangle: $L = 20$). The estimates based on Eq. (35) are shown by purple empty triangles. The phase diagram of the homogeneous system is also drawn with green empty squares.

close to the tip of the lobe. This is because the maximum of $\kappa_{\rm diff}(r)$ becomes very broad and finite-size effects are stronger. In that regime, one also needs a higher accuracy in the determination of the density in order to accurately compute the local compressibility. In spite of this, in 3D, the method based on the local compressibility yields more accurate results than in 2D (compare Figs. 9 and 11).

V. CONCLUSIONS

We have presented a detailed study of the finite-temperature phase diagram of strongly correlated bosons in the hard-core limit (or the XY model) in two and three dimensions. The critical parameters in the homogeneous case were determined through a finite-size scaling analysis of the superfluid stiffness and the condensate fraction. We introduced an approach to estimate the critical temperature from measurements of n_0 in finite systems. It makes use of the behavior of the derivative dn_0/dT and we derived finite-size scaling relations that can be used to extrapolate the results to the thermodynamic limit. This approach can be applied to systems that exhibit a diverging zero-momentum occupation in any dimension, irrespective of the universality class to which the transition belongs. We showed that this method is also accurate in 2D, where the system does not exhibit BEC. Furthermore, we computed the phase diagram using mean-field theory and found it to be quantitatively quite different from the results of numerically exact QMC simulations in 2D and 3D. Hence, for this model, thermal and quantum fluctuations are strong even in three dimensions, and mean-field theory is a poor approximation.

In the presence of an additional confining potential, we proved that the Bose-Hubbard model does not exhibit finite-temperature BEC in two dimensions, provided that density remains finite across the entire system in the thermodynamic

limit. Moreover, we considered measurements of the critical temperature and chemical potential of the homogeneous system based on experimentally measurable quantities such as the momentum distribution function and the local density profile. The accuracy of each method discussed depends on the dimensionality of the system and the range of temperatures and chemical potentials considered. In two dimensions, we found that the approach introduced in this work, based on the derivatives of n_0 with respect to β, is accurate in all regions of the phase diagram. A method based on the measurement of the local density was found to be reliable when T_c is low, while close to the tip of the superfluid lobe this approach is less effective, even when the trap is very shallow. This can be understood to be due to the strong deviations from the LDA close to the tip of the superfluid lobe. A quantitative account of these deviations based on trapped finite-size scaling, as presented in Ref. [85,86], would in principle allow one to perform an accurate size-scaling analysis in the presence of the confining potential, which might potentially improve the capabilities of the methods based on the measurements of the density profile. The accuracy of the latter method improves in 3D, but still remains inadequate as one approaches the tip of the superfluid lobe. In three dimensions, the approach based on $Q(T)$ was found to be the most accurate.

APPENDIX: DIFFERENCES BETWEEN dn_0/dT AND $dn_0/d\beta$

We briefly illustrate, by means of a simple analysis, why the estimate of the critical temperature based on dn_0/dT differs from the estimate based on $dn_0/d\beta$. We also discuss under which conditions the two estimates should approach each other.

We consider $n_0(\beta)$ to be the zero-momentum occupation in the vicinity of β_c. Its first derivative, which exhibits a maximum at β^*, can be written as

$$\frac{dn_0}{d\beta} = d_0 + a(\beta - \beta^*)^2, \qquad (A1)$$

where the curvature of the parabola is $a < 0$, the height of the maximum is d_0, and β is assumed to be very close to β^*. If instead we now compute dn_0/dT, we anticipate a minimum of this function located at a temperature $T^* \neq 1/\beta^*$ given by

$$\frac{1}{T^*} = \frac{3a\beta^* - |a|\sqrt{\beta^{*2} - \frac{8d_0}{a}}}{4a}. \qquad (A2)$$

In general, the position of the minimum as a function of T depends on the position of the maximum β^*, its curvature a, and its height d_0. However, in the limit of very large system sizes and very shallow traps, one expects the maximum of the derivative $dn_0/d\beta$ to be very sharp. In our simple example, this regime corresponds to a large value of the curvature, i.e., $|d_0/a| \ll \beta^{*2}$, which implies that $T^* \simeq 1/\beta^*$.

[1] J. G. Daunt and R. S. Smith, Rev. Mod. Phys. **26**, 172 (1954).

[2] C. Bruder, R. Fazio, and G. Schön, Phys. Rev. B **47**, 342 (1993).

[3] T. Giamarchi, C. Rüeg, and O. Tchernyshyov, Nature Phys. **4**, 198 (2008).

[4] I. Bloch, J. Dalibard, and W. Zwerger, Rev. Mod. Phys. **80**, 885 (2008).

[5] M. A. Cazalilla, R. Citro, T. Giamarchi, E. Orignac, and M. Rigol, Rev. Mod. Phys. **83**, 1405 (2011).

[6] M. P. A. Fisher, P. B. Weichman, G. Grinstein, and D. S. Fisher, Phys. Rev. B **40**, 546 (1989).

[7] D. Jaksch, C. Bruder, J. I. Cirac, C. W. Gardiner, and P. Zoller, Phys. Rev. Lett. **81**, 3108 (1998).

[8] T. Stöferle, H. Moritz, C. Schori, M. Köhl, and T. Esslinger, Phys. Rev. Lett. **92**, 130403 (2004).

[9] I. B. Spielman, W. D. Phillips, and J. V. Porto, Phys. Rev. Lett. **98**, 080404 (2007).

[10] K. Jiménez-García, R. L. Compton, Y.-J. Lin, W. D. Phillips, J. V. Porto, and I. B. Spielman, Phys. Rev. Lett. **105**, 110401 (2010).

[11] M. Greiner, O. Mandel, T. Esslinger, T. W. Hänsch, and I. Bloch, Nature (London) **415**, 39 (2002).

[12] S. Trotzky, L. Pollet, F. Gerbier, U. Schnorrberger, I. Bloch, N. V. Prokofev, B. Svistunov, and M. Troyer, Nature Phys. **6**, 998 (2010).

[13] V. Schweikhard, S. Tung, and E. A. Cornell, Phys. Rev. Lett. **99**, 030401 (2007).

[14] A. Trombettoni, A. Smerzi, and P. Sodano, New J. Phys. **7**, 57 (2005).

[15] X. Zhang, C.-L. Hung, S.-K. Tung, and C. Chin, Science **335**, 1070 (2012).

[16] G. G. Batrouni, V. Rousseau, R. T. Scalettar, M. Rigol, A. Muramatsu, P. J. H. Denteneer, and M. Troyer, Phys. Rev. Lett. **89**, 117203 (2002).

[17] M. Rigol, G. G. Batrouni, V. G. Rousseau, and R. T. Scalettar, Phys. Rev. A **79**, 053605 (2009).

[18] M. Rigol, A. Muramatsu, G. G. Batrouni, and R. T. Scalettar, Phys. Rev. Lett. **91**, 130403 (2003).

[19] S. Wessel, F. Alet, M. Troyer, and G. G. Batrouni, Phys. Rev. A **70**, 053615 (2004).

[20] M. Campostrini and E. Vicari, Phys. Rev. A **81**, 023606 (2010).

[21] M. Campostrini and E. Vicari, Phys. Rev. A **81**, 063614 (2010).

[22] P. Cladé, C. Ryu, A. Ramanathan, K. Helmerson, and W. D. Phillips, Phys. Rev. Lett. **102**, 170401 (2009).

[23] S. Tung, G. Lamporesi, D. Lobser, L. Xia, and E. A. Cornell, Phys. Rev. Lett. **105**, 230408 (2010).

[24] K. Xu, Y. Liu, D. E. Miller, J. K. Chin, W. Setiawan, and W. Ketterle, Phys. Rev. Lett. **96**, 180405 (2006).

[25] J. K. Chin, D. E. Miller, Y. Liu, C. Stan, W. Setiawan, C. Sanner, K. Xu, and W. Ketterle, Nature (London) **443**, 961 (2006).

[26] V. A. Kashurnikov, N. V. Prokofev, and B. V. Svistunov, Phys. Rev. A **66**, 031601(R) (2002).

[27] R. B. Diener, Q. Zhou, H. Zhai, and T.-L. Ho, Phys. Rev. Lett. **98**, 180404 (2007).

[28] Y. Kato, Q. Zhou, N. Kawashima, and N. Trivedi, Nature Phys. **4**, 617 (2008).

[29] L. Pollet, N. V. Prokofev, and B. V. Svistunov, Phys. Rev. Lett. **104**, 245705 (2010).

[30] S. Fölling, A. Widera, T. Müller, F. Gerbier, and I. Bloch, Phys. Rev. Lett. **97**, 060403 (2006).

[31] Q. Zhou, Y. Kato, N. Kawashima, and N. Trivedi, Phys. Rev. Lett. **103**, 085701 (2009).

[32] T.-L. Ho and Q. Zhou, Nature Phys. **6**, 131 (2010).

[33] S. Nascimbène, N. Navon, F. Chevy, and C. Salomon, New J. Phys. **12**, 103026 (2010).

[34] S. Fang, C.-M. Chung, P. N. Ma, P. Chen, and D.-W. Wang, Phys. Rev. A **83**, 031605(R) (2011).

[35] K. R. A. Hazzard, and E. J. Mueller, Phys. Rev. A **84**, 013604 (2011).

[36] N. Gemelke, X. Zhang, C.-L. Hung, and C. Chin, Nature (London) **460**, 995 (2009).

[37] J. F. Sherson, C. Weitenberg, M. Endres, M. Cheneau, I. Bloch, and S. Kuhr, Nature (London) **467**, 68 (2010).

[38] P. N. Ma, L. Pollet, and M. Troyer, Phys. Rev. A **82**, 033627 (2010).

[39] W. S. Bakr, A. Peng, M. E. Tai, R. Ma, J. Simon, J. I. Gillen, S. Folling, L. Pollet, and M. Greiner, Science **329**, 547 (2010).

[40] X. Zhang, C.-L. Hung, S.-K. Tung, N. Gemelke, and C. Chin, New J. Phys. **13**, 045011 (2011).

[41] E. Duchon, Y. Kato, and N. Trivedi, arXiv:1112.0592v1.

[42] P. Krüger, Z. Hadzibabic, and J. Dalibard, Phys. Rev. Lett. **99**, 040402 (2007).

[43] S. Nascimbène, N. Navon, K. J. Jiang, F. Chevy, and C. Salomon, Nature (London) **463**, 1057 (2010).

[44] C.-L. Hung, X. Zhang, N. Gemelke, and C. Chin, Nature (London) **470**, 236 (2011).

[45] N. D. Mermin, and H. Wagner, Phys. Rev. Lett. **17**, 1133 (1966).

[46] P. C. Hohenberg, Phys. Rev. **158**, 383 (1967).

[47] V. L. Berezinskii, Sov. Phys. JETP **34**, 610 (1972).

[48] J. M. Kosterlitz and D. J. Thouless, J. Phys. C **6**, 1181 (1973).

[49] Y.-H. Li and S. Teitel, Phys. Rev. B **40**, 9122 (1989).

[50] M. B. Salamon, J. Shi, N. Overend, and M. A. Howson, Phys. Rev. B **47**, 5520 (1993).

[51] N. Overend, M. A. Howson, and I. D. Lawrie, Phys. Rev. Lett. **72**, 3238 (1994).

[52] M. Campostrini, M. Hasenbusch, A. Pelissetto, and E. Vicari, Phys. Rev. B **74**, 144506 (2006).

[53] E. Burovski, J. Machta, N. Prokofev, and B. Svistunov, Phys. Rev. B **74**, 132502 (2006).

[54] M. Campostrini, M. Hasenbusch, A. Pelissetto, P. Rossi, and E. Vicari, Phys. Rev. B **63**, 214503 (2001).

[55] M. Hasenbusch and T. Török, J. Phys. A: Math. Gen. **32**, 6361 (1999).

[56] T. Matsubara and H. Matsuda, Prog. Theor. Phys. **16**, 569 (1956).

[57] A. W. Sandvik, and J. Kurkijärvi, Phys. Rev. B **43**, 5950 (1991).

[58] A. W. Sandvik, J. Phys. A **25**, 3667 (1992).

[59] A. Dorneich and M. Troyer, Phys. Rev. E **64**, 066701 (2001).

[60] E. Loh, D. J. Scalapino, and P. M. Grant, Phys. Rev. B **31**, 4712 (1985).

[61] H.-Q. Ding and M. S. Makivić, Phys. Rev. B **42**, 6827 (1990).

[62] H.-Q. Ding, Phys. Rev. B **45**, 230 (1992).

[63] K. Harada and N. Kawashima, Phys. Rev. B **55**, R11949 (1997).

[64] E. L. Pollock and D. M. Ceperley, Phys. Rev. B **36**, 8343 (1987).

[65] P. Olsson, Phys. Rev. B **52**, 4526 (1995).

[66] H. Weber and P. Minnhagen, Phys. Rev. B **37**, 5986 (1988).

[67] Note that in Ref. [63], a more sophisticated fitting approach allowed them to obtain the critical value with a higher accuracy that the one we achieve here.

[68] M. Hasenbusch, J. Phys. A: Math. Gen. **38**, 5869 (2005).

[69] D. J. Amit, Y. Y. Goldschmidt, and S. Grinstein, J. Phys. A: Math. Gen. **13**, 585 (1980).

[70] R. Kenna and A. C. Irving, Phys. Lett. B **351**, 273 (1995).

[71] M. H. Pedersen and T. Schneider, Phys. Rev. B **53**, 5826 (1996).

[72] N. Kawashima, J. Phys. Soc. Jpn. **73**, 3219 (2004).

[73] R. G. Melko and D. J. Scalapino, Phys. Rev. B **71**, 094511 (2005).

[74] M. E. Fisher, M. N. Barber, and D. Jasnow, Phys. Rev. A **8**, 1111 (1973).

[75] N. Laflorencie, Europhys. Lett. **99**, 66001 (2012).

[76] O. Penrose and L. Onsager, Phys. Rev. **104**, 576 (1956).

[77] A. Pelissetto and E. Vicari, Phys. Rep. **368**, 549 (2002).

[78] K. Sheshadri, H. R. Krishnamurthy, R. Pandit, and T. V. Ramakrishnan, Europhys. Lett. **22**, 257 (1993).

[79] F. Dalfovo, S. Giorgini, L. P. Pitaevskii, and S. Stringari, Rev. Mod. Phys. **71**, 463 (1999).

[80] W. J. Mullin, J. Low Temp. Phys. **106**, 615 (1997).

[81] R. A. Horn and C. R. Johnson, *Matrix Analysis* (Cambridge University Press, New York, 1985).

[82] C. E. Campbell, K. E. Kürten, M. L. Ristig, and G. Senger, Phys. Rev. B **30**, 3728 (1984).

[83] F. Alet, S. Wessel, and M. Troyer, Phys. Rev. E **71**, 036706 (2005).

[84] Q. Zhou, Y. Kato, N. Kawashima, and N. Trivedi, Phys. Rev. Lett. **105**, 199602 (2010).

[85] G. Ceccarelli, C. Torrero, and E. Vicari, Phys. Rev. A **85**, 023616 (2012).

[86] G. Ceccarelli and C. Torrero, Phys. Rev. A **85**, 053637 (2012).